UNIVERSITY of York

This is a repository copy of *Hybrid Metalens for Miniaturised Ultraviolet Fluorescence Detection*.

White Rose Research Online URL for this paper:
https://eprints.whiterose.ac.uk/203194/

Version: Published Version

Article:
Li, Kezheng, Martins, Augusto, Bohora, Sanket et al. (3 more authors) (2023) Hybrid Metalens for Miniaturised Ultraviolet Fluorescence Detection. Advanced Optical Materials. 2300852. ISSN 2195-1071

https://doi.org/10.1002/adom.202300852

Reuse
This article is distributed under the terms of the Creative Commons Attribution (CC BY) licence. This licence allows you to distribute, remix, tweak, and build upon the work, even commercially, as long as you credit the authors for the original work. More information and the full terms of the licence here: https://creativecommons.org/licenses/

Takedown
If you consider content in White Rose Research Online to be in breach of UK law, please notify us by emailing eprints@whiterose.ac.uk including the URL of the record and the reason for the withdrawal request.

White Rose university consortium
Universities of Leeds, Sheffield & York

eprints@whiterose.ac.uk
https://eprints.whiterose.ac.uk/

Check for updates

ADVANCED OPTICAL MATERIALS
www.advopticalmat.de

Hybrid Metalens for Miniaturised Ultraviolet Fluorescence Detection

Kezheng Li, Augusto Martins, Sanket Bohora, Ashim Dhakal, Emiliano R. Martins, and Thomas F. Krauss*

The advantages of metalenses to enable miniaturized systems have been well established, especially in the visible and infrared wavelength regimes. The ultraviolet (UV) presents a final frontier because feature size scales as the wavelength, so realizing a large size metalens with a high numerical aperture (NA) in the UV is a major challenge. Here, a single-layer, thin-film (450 nm) hybrid metalens with an NA of 0.9 and a diameter of 6.2 mm is presented. By combining a Fresnel lens and optimised binary gratings, the well-known shadowing effect of Fresnel lenses at high NA is avoided while being able to realize a large area lens. It is demonstrated that the combination of high NA and large area affords efficient detection of tryptophan-like fluorescence, which is a well-studied proxy for water contamination with faecal coliforms. The detection of tryptophan at levels better than 1 ppb, which corresponds to the low-risk category for drinking water according to the World Health Organization (WHO), is shown. It is also confirmed that the hybrid metalens fluorescence collection efficiency is 3.5 times higher than a high NA plano-convex lens used in state-of-the-art fluorometers, which demonstrates that the versatile metalens approach opens up new opportunities in the UV.

1. Introduction

The metalens paradigm, whereby a planar nanostructured surface manipulates an incoming wavefront for novel focusing and imaging functions, is one of the most exciting developments in Optics and Photonics in recent years. Because of their ability to miniaturize optical systems, such as smartphone lenses, metalenses were recognized as one of the top 10 emerging technologies by the World Economic Forum in 2019. The ability to miniaturize and create a step-change in optical system design is based on the metalens' wavelength-scale thickness and planarity, and the fact that they can be created by the same lithographic process irrespective of the complexity of the phase front they impose. These advantages have motivated a large amount of research that has led to many exciting developments in the visible and infrared wavelength range.[1-6] The ultraviolet (UV) regime, however, has seen much less activity. Metalenses are typically made up of "meta-atoms", i.e., photonic nanostructures that control the response of the lens on a sub-wavelength scale. As the wavelength gets shorter, it becomes ever more difficult to make the required sub-wavelength structures; moreover, the choice of UV-compatible materials is very limited and the sheer number of meta-atoms that need to be manipulated by the lithographic system limits the ability to create large lenses. As a result, very few metalenses that operate in the UV have been presented, and none of them are larger than 500 µm in diameter.[7-10] Such small lenses are not suitable for the very important application of fluorescence collection in a practical system.

Here, we introduce a novel hybrid design overcoming these issues and enabling the demonstration of efficient UV (350 nm) fluorescence collection. Our design paves the way towards a truly miniaturized fluorescence detection system, because it enables the replacement of currently used bulk lenses by a much smaller, yet more efficient, approach, as demonstrated below. The metalens design is based on the combination of a thin-film Fresnel lens with a circular binary grating lens in a single, wavelength-scale layer, exploiting the following insights:

a) Fresnel lenses are known to be very efficient and can be readily produced lithographically, using "grey-scale" lithography.

K. Li, T. F. Krauss
School of Physics
Engineering and Technology
University of York
York YO10 5DD, UK
E-mail: kezheng.li@york.ac.uk

A. Martins
Department of Physics
Harvard University
Cambridge, MA 02138, USA

S. Bohora, A. Dhakal
Biophotonics Lab
Phutung Research Institute
Tarakeshor-7, Kathmandu 44611, Nepal

E. R. Martins
São Carlos School of Engineering
Department of Electrical and Computer Engineering
University of São Paulo
São Paulo 13566–590, Brazil

The ORCID identification number(s) for the author(s) of this article can be found under https://doi.org/10.1002/adom.202300852

© 2023 The Authors. Advanced Optical Materials published by Wiley-VCH GmbH. This is an open access article under the terms of the Creative Commons Attribution License, which permits use, distribution and reproduction in any medium, provided the original work is properly cited.

DOI: 10.1002/adom.202300852

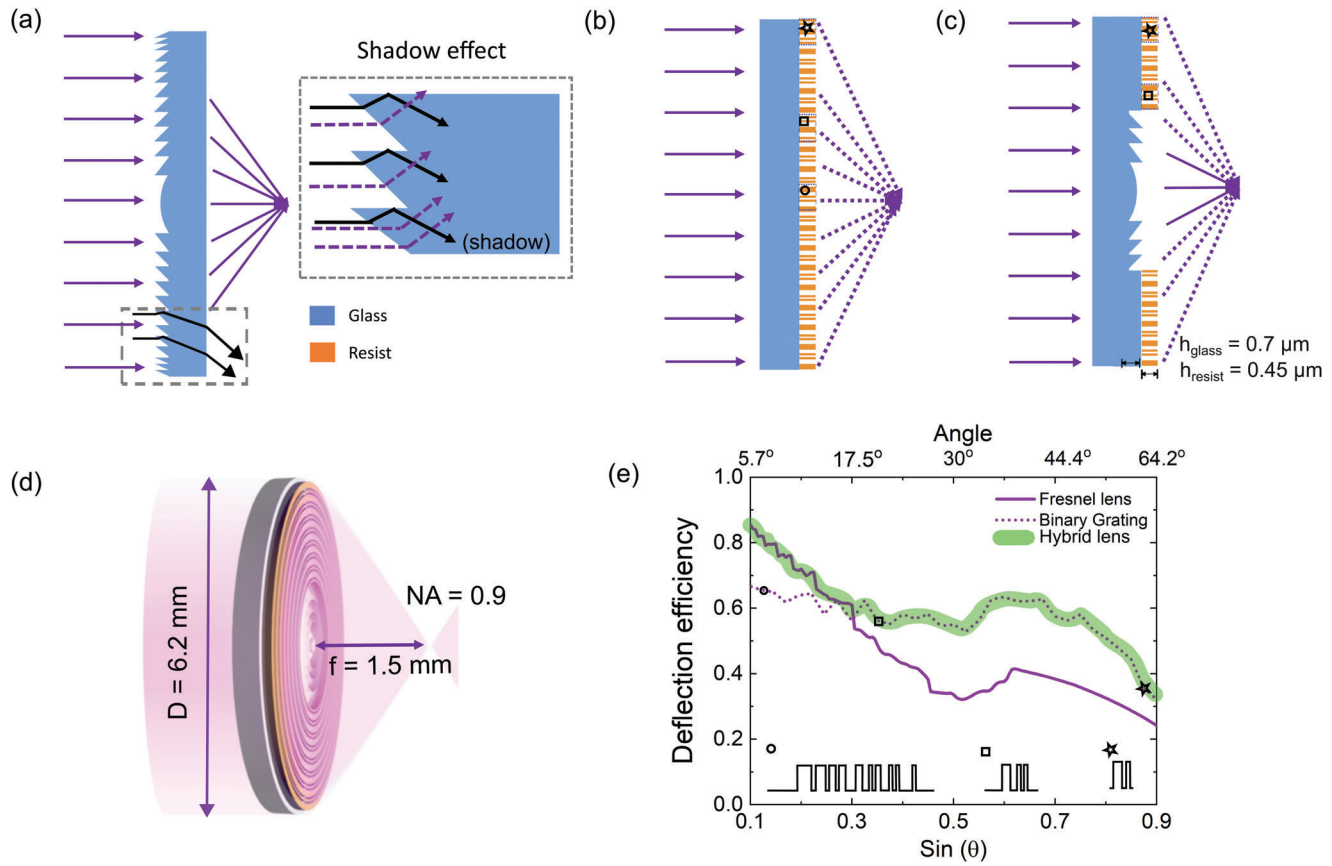

Figure 1. Working principle of a hybrid metalens. a-c) Cross section of the Fresnel lens, binary grating lens, and hybrid lens structure. The solid purple lines indicate the incident and deflected rays from the Fresnel lens, while the dashed lines indicate the diffracted rays from the binary grating lens. The inset of (a) illustrates the shadowing effect. d) 3D sketch of the hybrid metalens working at a wavelength of 350 nm with a diameter of 6.2 mm and NA of 0.9. e) The efficiency as a function of deflection angle and numerical aperture for the above-mentioned lenses. The deflection efficiency of the Fresnel lens is calculated for a minimum feature size of 200 nm. The inset shows the height profiles of the optimized binary lens at different deflecting angles (NAs). The film's height is 450 nm with a minimum feature size of 75 nm for the binary grating.

Their efficiency, however, rapidly drops with increasing numerical aperture due to the "shadowing effect"[11] and increased Fresnel reflections; thus, they are not suitable for high NA operation.

b) The phase change imposed by meta-atoms can also be generated by a circular binary grating; the trade-off is efficiency, but such binary gratings can be fabricated on a smaller scale, suitable for operation in the UV. They are also largely polarisation-independent, in contrast to many meta-atom designs, which is an essential feature for high-efficiency fluorescence collection.

Our hybrid design bypasses the shadowing effect problem of Fresnel lenses by combining them with binary gratings, thus leading to flat lenses maintaining high efficiency in the high areas and NAs regime. Thus, the hybrid designs introduce flat lenses also into the UV range, which is the relevant domain to applications such as medical fluorescence endoscopy, remote inspection in industry, and water contamination testing. In those applications, conventional metalens designs are not suitable because of their small areas while refractive lenses are too bulky, limiting opportunities for miniaturization.

2. Results

Figure 1a–c depicts a Fresnel lens, a binary lens, and a hybrid lens, respectively. The Fresnel lens is placed with its structured side facing the plane wave source for focusing. Due to the discontinuity at every 2π phase step, the lens pattern introduces a "shadow" that deflects light into spurious orders for large deflection angles (inset of Figure 1a), which decreases the efficiency as a function of numerical aperture. For a more detailed explanation of this "shadowing" effect, see Section S3 of Supporting Information (SI). Figure 1e shows the deflection efficiency of the different lenses, the solid and dashed lines representing the Fresnel and the binary lens, respectively. The deflection efficiency is defined as the first-order diffraction efficiency of a periodic blazed grating based on the multilevel Fresnel lens design and of each optimized binary grating (details in Methods section and Supporting Information Section S6). At low deflection angles, the Fresnel design achieves higher diffraction efficiencies, but the shadowing effect quickly kicks in and reduces the efficiency with increasing deflection angle.[11] In contrast, the binary lens maintains its efficiency into higher angles, although it performs worse than the Fresnel lens at low angles. The cross-over between the Fresnel lens and

© 2023 The Authors. Advanced Optical Materials published by Wiley-VCH GmbH

21951071, 0, Downloaded from https://onlinelibrary.wiley.com/doi/10.1002/adom.202300852 by Test, Wiley Online Library on [08/09/2023]. See the Terms and Conditions (https://onlinelibrary.wiley.com/terms-and-conditions) on Wiley Online Library for rules of use; OA articles are governed by the applicable Creative Commons License

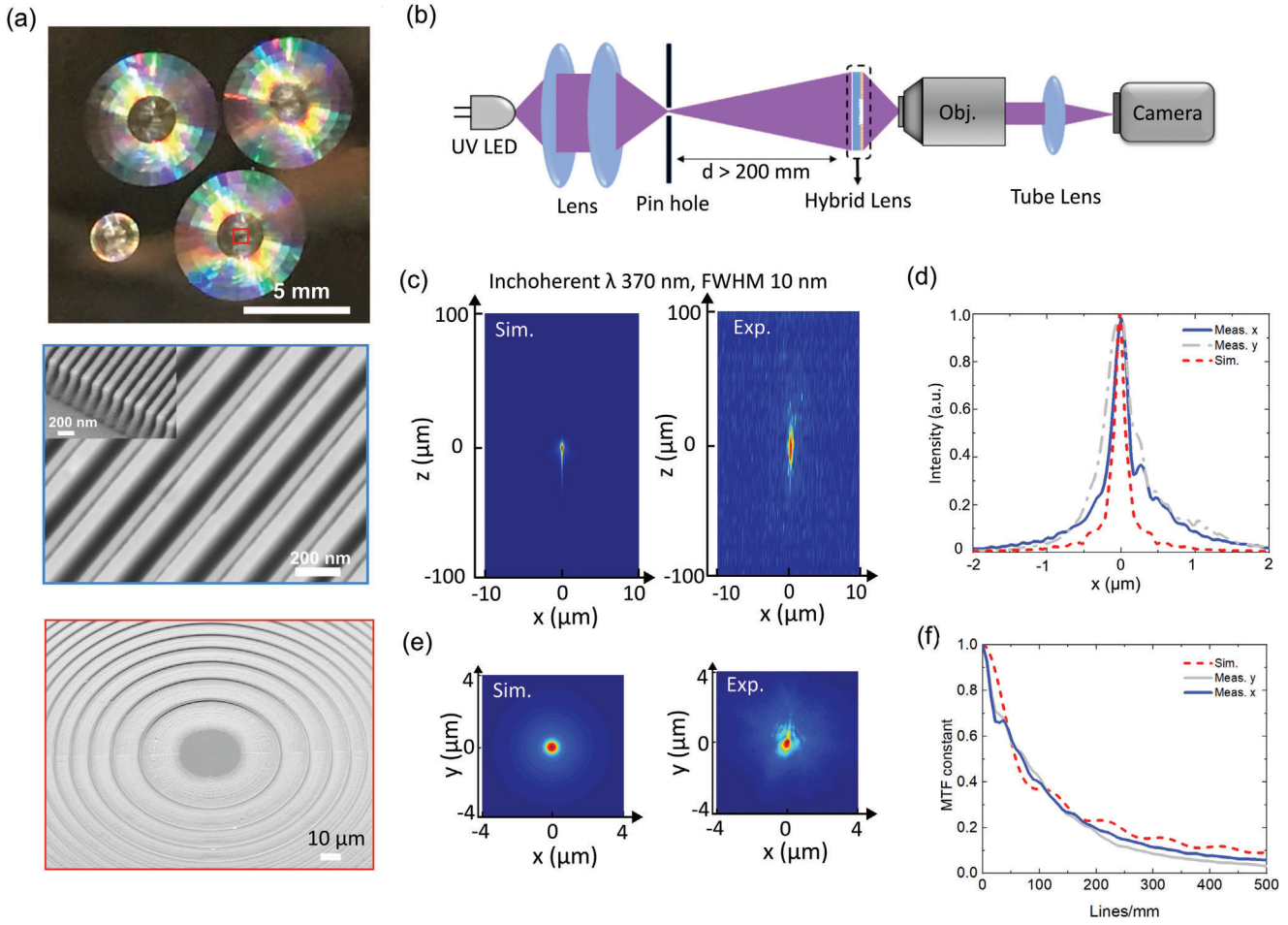

Figure 2. Hybrid lens and characterization of its focusing behavior. a) Photograph of a variety of flat lenses fabricated on a borofloat glass substrate. Hybrid lenses (NA = 0.9) are located on top left and bottom right of the photograph; the binary-only lens is located on the top right and the smaller lens on the bottom left is a Fresnel lens. Middle and bottom picture: SEM images of the outer and inner parts of the hybrid lens. b) Optical setup for characterizing the point spread function (PSF). c) Simulated and measured PSF along the optical axis of the hybrid lens. d) The dashed red curve represents the simulated focal spot profile and the blue and grey curves represent the measured spot profile along the longitudinal and the transversal directions. e) Intensity distribution of the focal spots by simulation and measurement. f) Modulation transfer function (MTF) for simulated and measured focal spots.

the binary lens efficiency occurs at an angle of 21° (sin (θ) ≅ 0.36); we, therefore, used this value in our design and implemented a Fresnel pattern in the center of the lens and a binary grating outside the radius that corresponds to NA > 0.36. The deflection efficiency of the hybrid lens is presented as the green curve in Figure 1e. We designed a hybrid lens with an NA of 0.9, (diameter 6.2 mm, focal length 1.5 mm) operating at a wavelength of 360 nm.

The difference between the various lenses were demonstrated by fabricating each design. We chose a maximum value of NA = 0.9, which is important for the fluorescence application; the largest NA of a Fresnel lens that an e-beam grayscale lithography system can achieve is ≈0.6,[12] so we also fabricated several lenses with this NA to quantify the gain obtained by the high NA (0.9) enabled by the hybrid design. All lenses have the same focal length of 1.5 mm with different diameters: 2.25 mm for NA of 0.6 and 6.2 mm for NA of 0.9. **Figure 2**a shows a photograph of the fabricated lenses and corresponding scanning electron micrographs (SEM) of binary lens, Fresnel lens, and hybrid lens. To assess the performance of the lenses, we measured their focusing efficiencies. We define focusing efficiency as the ratio of the focused optical power to the total power illuminating the lens (more details can be found in Section S4 of the Supporting Information). The Fresnel lens has an efficiency of 44.6%, whereas the binary and hybrid lenses have focusing efficiencies of 11.7% and 13.9%, respectively. Note that, even with the lower efficiency (13.9%) of the high NA (0.9) hybrid lens when compared to the efficiency (44.6%) of the lower NA (0.6) Fresnel lens (which we attribute to fabrication imperfections and the difficulty of making high-quality nanostructures for the very short wavelengths required here) the hybrid lens still significantly outperforms both the Fresnel lens and the type of bulk lenses used in state-of-the-art fluorometers (see **Figure 3**b). Finally, in addition to the higher efficiency provided by the hybrid lens, it requires less time for e-beam exposure compared to the binary grating lens, making it a more time-efficient option in terms of fabrication. Additionally,

© 2023 The Authors. Advanced Optical Materials published by Wiley-VCH GmbH

21951071, 0, Downloaded from https://onlinelibrary.wiley.com/doi/10.1002/adom.202300852 by Test, Wiley Online Library on [08/09/2023]. See the Terms and Conditions (https://onlinelibrary.wiley.com/terms-and-conditions) on Wiley Online Library for rules of use; OA articles are governed by the applicable Creative Commons License

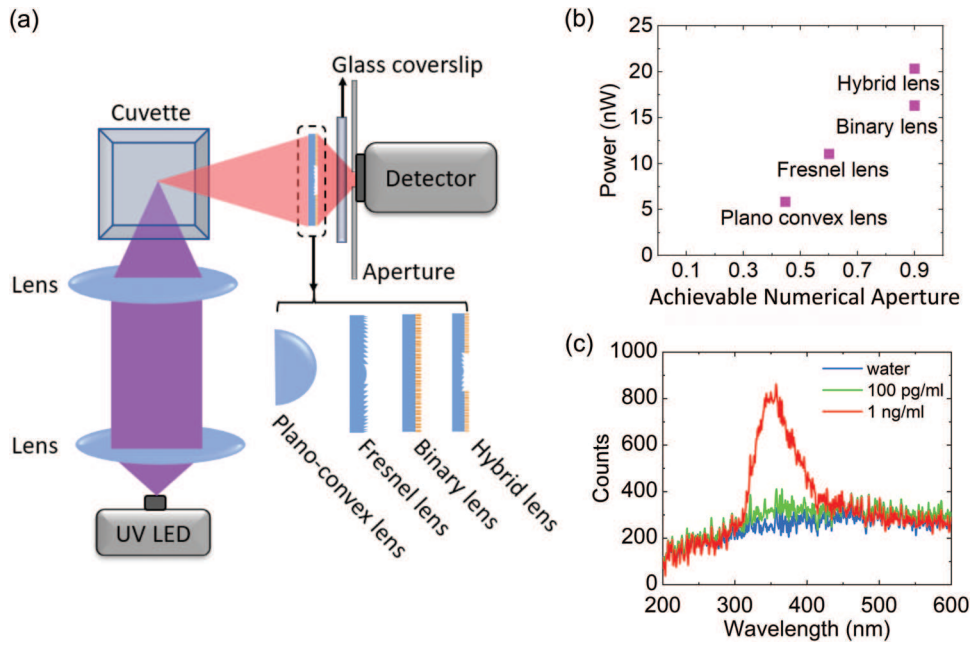

Figure 3. Tryptophan fluorescence measurement. a) Fluorescence detection setup. b) Absolute power collected by plano-convex lens, Fresnel lens, binary lens, and hybrid lens for a tryptophan concentration of 1 mg ml^{-1}. The error bars are all near 0.05 nW, which is not visible in this plot. c) Fluorescence spectrum collected by the hybrid lens for different concentrations of tryptophan with an integration time of 10 s.

the hybrid lens exhibits reduced polarization dependence, which is advantageous for power collection purposes, because the Fresnel lens section does not exhibit polarization dependence. Finally, we envision that such a lens might be reproduced by nanoimprint lithography, in which case the Fresnel and binary grating sections can be reproduced in a single step.

In order to further understand the focusing behavior of the hybrid lens, we simulated and experimentally obtained its point spread function (PSF) and modulation transfer function (MTF). Figure 2b shows the setup used for the PSF characterization. We imaged a 10 μm pinhole placed at ≈200 mm from the lens that was illuminated with focused light from a 370 nm LED with 10 nm linewidth of the spectrum. Figure 2c,d,e show the longitudinal and transversal cuts of the point spread function, respectively. Figure 2e shows the corresponding MTFs. Note the good agreement between the measured and simulated results. We also analyzed the fabrication error regarding the center lateral misalignment and focal lengths variation. The results show stable operation and limited performance variations, highlighting the stability of our design to fabrication imperfections, especially for nonimaging applications (more details are shown in Section S5 of Supporting Information). Another aspect worth mentioning is that the simplicity of the binary grating design allows us to generate features on a smaller scale (smallest feature size of 75 nm), over a larger area, and with faster speed (Section S7 of Supporting Information) compared to a typical metaatom design, which are the key reasons why this design is practically feasible and suitable for fluorescence applications in the UV.

In order to test the various lenses and demonstrate the superiority of the hybrid lens and its suitability for real-world applications, we carried out a series of fluorescence experiments. We used tryptophan as the model fluorophore, because of its importance in indicating drinking water quality; the relationship between tryptophan-like fluorescence and the presence of fecal coliforms in drinking water has now been confirmed by a number of studies.[13–17] The concentration of tryptophan that corresponds to safe drinking water levels according to the World Health Organisation (WHO) is on the order of 1 ppb (1 ng ml^{-1}).[18]

We used tryptophan solutions of concentrations starting from 100 pg ml^{-1} (0.1 ppb) up to 1 mg ml^{-1}. The fluorescence was recorded with the setup shown in Figure 3a. Tryptophan is typically excited at 275 nm and emits at 340 nm.[13] We used a UV LED (Inolux, IN-C39ATKU1CT-ND, central wavelength 275 nm, 0.2 mW, see also Supporting Information, Section S2) and focused it into a UV fused quartz cuvette (CV10Q14, Thorlabs) containing the tryptophan solution. The fluorescence signal is collected by the various lenses and fed into a UV power meter (Gentec-e, Pronoto) and a spectrometer (LR1, ASEQ instruments). We used the following lenses for the comparison: A hybrid lens (NA = 0.9), a binary grating lens (NA = 0.9), a Fresnel lens (NA = 0.6), and finally, a plano-convex quartz lens for comparison – with the largest NA available on the market, i.e., NA = 0.447. We note that the plano-convex lens represents the highest NA lens used in practical fluorometers, for reasons of size and cost, and is, therefore, a fair comparison for the application considered here. As an excitation filter, we used a glass coverslip. We did not use an emission filter, as tryptophan was the only source of fluorescence in the system as confirmed by the spectrum in Figure 3c.

Figure 3b summarizes the collected fluorescence power as a function of NA, with each data point representing a different type of lens. For this measurement, we used a tryptophan

© 2023 The Authors. Advanced Optical Materials published by Wiley-VCH GmbH

21951071, 0, Downloaded from https://onlinelibrary.wiley.com/doi/10.1002/adom.202300852 by Test, Wiley Online Library on [08/09/2023]. See the Terms and Conditions (https://onlinelibrary.wiley.com/terms-and-conditions) on Wiley Online Library for rules of use; OA articles are governed by the applicable Creative Commons License

concentration of 1 mg ml^{-1} to ensure a strong signal for ease of comparison. The advantage of the higher NA achieved by the hybrid metalens is readily appreciated from this result. We also note that all other planar lenses outperformed the plano-convex lens due to their higher NA, despite having lower focusing efficiencies. The plano-convex lens collected 5.84 nW of power, which is approximately half of the power collected by the Fresnel lens (11.05 nW) and <30% of that collected by the hybrid lens (20.32 nW).

Finally, we confirmed the suitability of the hybrid lens fluorescence setup to detect tryptophan-like fluorescence (TLF) at WHO drinking water levels. The spectral measurements clearly demonstrate the ability of the hybrid lens setup to collect a fluorescence signal at a very low concentration of 1 ng ml^{-1} (1 ppb) (red line in Figure 3c); there is even a detectable 350 nm fluorescence signal at 0.1 ppb (green line in Figure 3c), which is therefore close to or just below the limit of detection; in any case, the ability to detect a 1 ppb signal (red line in Figure 3c) is clearly evident. Therefore, the hybrid lens approach has clearly demonstrated its superiority over other approaches, including a bulk lens, and its ability to detect fluorescence at levels suitable for real-world applications. Besides that, the hybrid lens offers the opportunity to build other miniaturized fluorometers to be integrated into medical endoscopes, remote inspection tools for industry, or water quality testing applications where current fluorometers are too expensive and bulky.

These results highlight the remarkable flexibility of the flat optics design over traditional refractive bulk lenses. We also note that high NA refractive lenses require aspheric designs, which demands complex and expensive mechanical tools for precise shaping of the glass surface. In contrast, flat lenses can achieve a high NA simply by design, and the parameters used here are all within the capability of nanoimprint lithography, so the lens could be replicated at a low cost. Naturally, the strategy we describe is also applicable for the visible regime, where even larger lenses can be realized for efficient fluorescence collection in space-constrained systems. For example, many fluorescent dyes used in life science, such as green fluorescence protein and rhodamine, could be detected by such lenses. More details can be found in Supporting Information Section S6.

3. Conclusion

We have demonstrated a novel design method to achieve high NA hybrid metalenses operating in the UV region. The design combines the high efficiency of Fresnel lenses for low deflection angles with the superior deflection efficiency of binary grating at higher angles. We demonstrate a hybrid metalens with an NA of 0.9 and apply it to the important problem of UV fluorescence collection. Using fluorescence from tryptophan solutions, which is relevant to the contamination of drinking water, we show that our metalens collects 3.5 times more fluorescent UV light than a standard plano-convex lens and importantly, it offers the prospect for a low-cost, miniaturized fluorometer operating in the UV. To the best of our knowledge, this is the first demonstration of a metalens of practical area operating in the UV region and demonstrating efficient fluorescence collection. While this work was aimed at light collection, we note that the point spread functions we show experimentally also make our hybrid lens design suitable for imaging applications. Therefore, our work paves the way for metalens applications in the UV spectral region, especially for the design of miniaturized fluorescent systems, but importantly, also for achieving large area metalenses for imaging applications at other wavelengths.

4. Experimental Section

Multilevel Fresnel Lens Design: The Fresnel lens section was etched into a Borofloat (Schott.com) glass substrate using grey-scale lithography and reactive ion etching (RIE) to a maximum depth of 700 nm. Borofloat glass has a refractive index of 1.47 and low losses at 350 nm in wavelength. The binary grating was created in a 450 nm thin layer of ma-N 2403 (Microresist, GmbH) by direct electron-beam writing. The refractive index of ma-N 2403 is 1.7 at 350 nm and has negligible absorption at that wavelength (Section 1 of Supporting Information). Two different resists needed to be used to realize the two sections because the requirements were very different. For the Fresnel section, we used PMMA 950, because it allows for a good control over the greyscale. The ma-N 2403 used for the binary grating, in contrast, exhibits a steep sensitivity curve, where very small variations of the electron beam dose lead to significant differences in the height profile, which is ideal for a binary profile. Regarding the phase profile, the hybrid lens is designed. To avoid spherical aberrations, the hybrid lens is designed to modulate the wavefront with the well-known hyperbolic phase profile, shown in Equation (1).

$$\varphi(r) = -k_0 n_{\text{ext}}\left(\sqrt{f^2 + r^2} - f\right) + \pi \tag{1}$$

where r is the radial coordinate, f the focal length, $k_0 = 2\pi/\lambda_0$ the free space wavenumber and n_{ext} the refractive index of the focusing medium. The Fresnel lens height profile was generated following the same approach as in[19] using a multilevel approach with a minimum width resolution of 200 nm. This resolution was imposed by taking into consideration of the lateral step size (20 nm to guarantee a sufficient etching mask) of the lithographic system. Given this technological limitation, the maximum NA of a multilevel Fresnel lens is 0.6 at 350 nm.

The Fresnel lens design modulates the transmitted wavefront with the hyperbolic phase profile $\phi(r)$, First, the phase profile was kept to the [0,2π) branch

$$\phi'(r) = \arg e^{i\phi(r)} + \pi \tag{2}$$

The phase profile is then quantized into M levels by the following equation

$$\phi'_S(r) = \text{round}\left(\frac{\phi'(r)}{2\pi} M\right) * \frac{2\pi}{M} \tag{3}$$

where round is the rounding to the nearest integer function. The phase sampling was performed with a different number of levels in order to keep the minimum resolution larger than 200 nm. Therefore, the phase profile was split into N equally spaced regions $[r_i, r_{i+1})$, where $i \in \{1, 2, \ldots N\}$, $r_i = \frac{(i-1)R}{N}$ and R is the Fresnel lens radius. Therefore, within each region, the number of phase levels (M) was chosen to keep the minimum width of each phase level plateau >200 nm.

Binary Lens Design: The binary lens design was based on a supercell approach that samples the phase profile gradient instead of its local phase value.[20] This means that, for a given radius r_i, the grating was optimized such that its lattice vector G matches the phase profile gradient at that point, as shown in Equation (4)

$$G = \frac{2\pi}{a} = \frac{d\varphi(r)}{dr} \tag{4}$$

© 2023 The Authors. Advanced Optical Materials published by Wiley-VCH GmbH

21951071, 0, Downloaded from https://onlinelibrary.wiley.com/doi/10.1002/adom.202300852 by Test, Wiley Online Library on [08/09/2023]. See the Terms and Conditions (https://onlinelibrary.wiley.com/terms-and-conditions) on Wiley Online Library for rules of use; OA articles are governed by the applicable Creative Commons License

where *a* is the supercell period. The grating height is fixed at 450 nm to impose the required phase change. The first-order deflection efficiency is optimized via a binary search algorithm combined with the rigorous coupled wave analysis method.[21] In the optimization process, the minimum ridge and width sizes were limited to 75 nm as this was the smallest size that could reliably produce with the lithographic process.

The binary outer region could also be based on a 2D meta-atom design, which was typically used for metalenses due to its polarization insensitivity. However, the relatively low refractive index of the ma_N 2403 and the very short operating wavelength demand very small feature sizes and high aspect ratios that were extremely difficult to fabricate consistently. Instead, the binary ring design chosen was slightly easier to fabricate. Therefore, it was noted that the binary grating approach offers a suitable compromise between feasibility and performance. Additionally, a lens consisting of 2D meta-atoms would require a significantly longer writing time. (See Section S7 of Supporting Information).

Fresnel Lens Fabrication: PMMA 950 (MicroResist) was spin-coated on a 500 µm thick Borofloat (Schott.com) glass substrate, and a charge dissipation layer AR-PC 5090 (Allresist GmbH) is coated on top to prevent a charging effect. Then e-beam lithography was employed to define the grayscale Fresnel patterns on PMMA, followed by the development of a mixture solution of deionised (DI) water: isopropanol (IPA) of 3:7. Subsequently, reactive ion etching (RIE) was performed to transfer the pattern from PMMA to Borofloat glass substrate. Finally, the remaining PMMA resist was removed in acetone.

Binary Grating Fabrication: The negative electron-beam resist ma-N 2403 (MicroResist, GmbH) is spin-coated onto a Borofloat glass substrate, on top of which a charge dissipation layer AR-PC 5090 (Allresist GmbH) was coated to prevent a charging effect. Then e-beam lithography was employed to define the binary gratings on the ma-N layer, followed by development in the developer of Ma-D 525 (Allresist GmbH).

Hybrid Lens Fabrication: The hybrid lens was fabricated by overlaying the binary grating onto a predefined Fresnel lens. The procedure was a combination of the procedures described above.

Deflection Efficiency Simulations: The deflection efficiency was defined as the first-order diffraction efficiency of a periodic blazed grating based on each design. That is, the multilevel Fresnel lens, it corresponds to a multilevel blazed grating whose period was adjusted for the required deflection angle according to the grating equation. For the ma-N 2403-based binary gratings, it corresponds to the diffraction efficiency of each optimized grating. Both were simulated using an unpolarized normal incident planewave from the glass substrate. The first-order diffraction efficiency was defined as the power going to the first order with respect to the incident power. All simulations were performed using the rigorous coupled wave analysis method.

Optical Setup: The optical setup for characterizing the point spread function of the hybrid lens is illustrated in Figure 2b. A point source was created by placing a pair of lenses between a UV LED (Marktech Optoelectronics, MTE3661N1-UV) and a pinhole with a 10 µm diameter. The distance between the pinhole and the hybrid lens is >200 mm which gives a small divergence angle (15 mrad). In this case, the imaging size of the pinhole was <100 nm, which was smaller than the hybrid lens' resolution, so it can be treated as a point source. The 50x objective lens was placed on the linear transition stage to adjust the distance from the flat lenses. A tube lens with a focal length of 75 mm was placed before the camera (Raspberry Pi Camera Module 2 NoIR).

Tryptophan Solution Preparation: Tryptophan (L-Tryptophan, L-α-Amino-3-indolepropionic acid, (S)−2-Amino-3-(3-indolyl) propionic acid, C11H12N2O2, CAS: 73-22-3) was purchased from Sigma-Aldrich Merck KGaA. Then diluted in DI water into different concentrations.

Supporting Information

Supporting Information is available from the Wiley Online Library or from the author.

Acknowledgements

This work was supported by the Engineering and Physical Research Council (EPSRC)'s Global Challenges Research Fund (GCRF) of the UK government under Grants EP/T020008/1, EP/W524165/1, and EP/P030017/1 and by The World Academy of Sciences (TWAS) and SIDA's grant No. 18-013 RG/PHYS/AS_I. E.R.M. acknowledges the São Paulo Research Foundation FAPESP (grants 2020/00619-4, 2021/06121-0) and CNPQ grant 307602/2021-4. A.D. acknowledges the Optica Foundation's 20th Anniversary Challenge Prize.

Conflict of Interest

The authors declare no conflict of interest.

Author Contributions

K.L. and A.M. contributed equally to this work.

Data Availability Statement

The data that support the findings of this study are available on request from the corresponding author. The data are not publicly available due to privacy or ethical restrictions.

Keywords

fluorescence, Fresnel lens, Metalens, ultraviolet, water

Received: April 11, 2023
Revised: June 12, 2023
Published online:

[1] M. Khorasaninejad, W. T. Chen, R. C. Devlin, J. Oh, A. Y. Zhu, F. Capasso, *Science* **2016**, *352*, 1190.
[2] A. Martins, K. Z. Li, J. T. Li, H. W. Liang, D. Conteduca, B.-H. V. Borges, T. F. Krauss, E. R. Martins, *ACS Photonics* **2020**, *7*, 2073.
[3] J. Engelberg, C. Zhou, N. Mazurski, J. Bar-David, A. Kristensen, U. Levy, *Nanophotonics* **2020**, *9*, 361.
[4] M. K. Chen, Y. Wu, L. Feng, Q. Fan, M. Lu, T. Xu, D. P. Tsai, *Adv. Opt. Mater.* **2021**, *9*, 2001414.
[5] R. Sawant, D. Andrén, R. J. Martins, S. Khadir, R. Verre, M. Käll, P. Genevet, *Optica* **2021**, *8*, 1405.
[6] D. Andren, J. Martinez-Llinas, P. Tassin, M. Kall, R. Verre, *ACS Photonics* **2020**, *7*, 885.
[7] Y. Deng, X. Wang, Z. Gong, K. Dong, S. Lou, N. Pégard, K. B. Tom, F. Yang, Z. You, L. Waller, J. Yao, *Adv. Mater.* **2018**, *30*, 1802632.
[8] K. Huang, J. Deng, H. S. Leong, S. L. K. Yap, R. B. Yang, J. Teng, H. Liu, *Laser Photonics Rev.* **2019**, *13*, 1800289.
[9] C. Zhang, S. Divitt, Q. Fan, W. Zhu, A. Agrawal, Y. Lu, T. Xu, H. J. Lezec, *Light Sci Appl* **2020**, *9*, https://doi.org/10.1038/s41377-020-0287-y.
[10] M. L. Tseng, M. Semmlinger, M. Zhang, C. Arndt, T. T. Huang, J. Yang, H. Y. Kuo, V.-C. Su, M. K. Chen, C. H. Chu, B. Cerjan, D. P. Tsai, P. Nordlander, N. J. Halas, *Sci. Adv.* **2022**, *8*, https://doi.org/10.1126/sciadv.abn5644.
[11] P. Lalanne, P. Chavel, *Laser Photonics Rev.* **2017**, *11*, 1600295.
[12] R. Kirchner, V. A. Guzenko, H. Schift, *Adv. Opt. Technol.* **2019**, *8*, 175.
[13] J. Bridgeman, M. Bieroza, A. Baker, *Rev. Environ. Sci. Bio/Technol.* **2011**, *10*, 277.

© 2023 The Authors. Advanced Optical Materials published by Wiley-VCH GmbH

21951071, 0, Downloaded from https://onlinelibrary.wiley.com/doi/10.1002/adom.202300852 by Test, Wiley Online Library on [08/09/2023]. See the Terms and Conditions (https://onlinelibrary.wiley.com/terms-and-conditions) on Wiley Online Library for rules of use; OA articles are governed by the applicable Creative Commons License

[14] S. Cumberland, J. Bridgeman, A. Baker, M. Sterling, D. Ward, *Environ. Technol.* **2012**, *33*, 687.
[15] A. Baker, S. A. Cumberland, C. Bradley, C. Buckley, J. Bridgeman, *Sci. Total Environ.* **2015**, *532*, 14.
[16] J. P. R. Sorensen, D. J. Lapworth, B. P. Marchant, D. C. W. Nkhuwa, S. Pedley, M. E. Stuart, R. A. Bell, M. Chirwa, J. Kabika, M. Liemisa, M. Chibesa, *Water Res.* **2015**, *81*, 38.
[17] S. Nowicki, D. J. Lapworth, J. S. T. Ward, P. Thomson, K. Charles, *Sci. Total Environ.* **2019**, *646*, 782.
[18] WHO Guidelines for Drinking Water Quality **2017**, WHO: Geneva, Switzerland, 2017, ISBN 9783540773405, https://www.who.int/publications/m/item/guidelines-for-drinking-water-quality-4th-ed.-incorporating-the-1st-addendum-(chapters).
[19] E. Noponen, J. Turunen, A. Vasara, *J. Opt. Soc. Am. A* **1993**, *10*, 434.
[20] C. Spägele, M. Tamagnone, D. Kazakov, M. Ossiander, M. Piccardo, F. Capasso, *Nat. Commun.* **2021**, *12*, https://doi.org/10.1038/s41467-021-24071-2.
[21] D. M. Whittaker, I. S Culshaw, *Phys. Rev. B* **1999**, *60*, 2610.

© 2023 The Authors. Advanced Optical Materials published by Wiley-VCH GmbH

21951071, 0, Downloaded from https://onlinelibrary.wiley.com/doi/10.1002/adom.202300852 by Test, Wiley Online Library on [08/09/2023]. See the Terms and Conditions (https://onlinelibrary.wiley.com/terms-and-conditions) on Wiley Online Library for rules of use; OA articles are governed by the applicable Creative Commons License